ORIGINAL PAPER

Antileukemic potential of PEGylated gold nanoparticle conjugated with protein toxin (NKCT1) isolated from Indian cobra (*Naja kaouthia*) venom

**Tanmoy Bhowmik · Partha Pratim Saha ·
Anjan Dasgupta · Antony Gomes**

Abstract Limited efficacy of current first-line treatment for leukemia calls attention for further development of efficient strategies. Recently, much attention has been given to nanoparticle-based drug delivery systems loaded with dual drugs to improve current disease therapies by overcoming toxicity. In the present study, we document to explore an approach to conjugate gold nanoparticles (GNPs) with protein toxin (NKCT1), a protein toxin from the Indian cobra (*Naja kaouthia*) venom, and to establish its antileukemic activity. GNP was prepared by $NaBH_4$ reduction method. UV–vis spectroscopy of GNP showed the absorbance at 530 nm for plasma resonance. Dynamic light scattering (DLS) size of GNPs was 2–8 nm and the GNP-NKCT1 was 68–122 nm. CD spectra of GNP-NKCT1 showed change in percentage of β-turn as compared with NKCT1. GNP-NKCT1 significantly inhibited leukemic cell growth in dose- and time-dependent manner by two- to threefold more than NKCT1. For human leukemic lymphoma cell line and human myelogenous leukemic cell line, the IC50 dose was found to be 1.2 and 0.75 μg/ml, respectively, observed by trypan blue exclusion method and tetrazolium bromide reduction assay. Flow cytometric analysis showed appreciable number of both cell lines in early and late apoptotic stages and arrested cell cycle in the G1 phase by GNP-NKCT1. Resilient power of leukemic cell line after wound healing and migration or invasive power of the cell line was significantly low in GNP-NKCT1-treated plate than the control plate. These analyses reveal that GNP-NKCT1 possesses significant and selective anticancer activity, likely by inducing programmed cell death through mitochondrial and/or lysosomal pathway.

Keywords GNP-NKCT1 · Nanoparticle · Leukemic cell · Apoptosis · Flow cytometry · Cell cycle

1 Introduction

Snake venoms contain a wide range of proteins and peptides (90–95 %), amino acids, nucleotides, free lipids, carbohydrates, and metallic elements bound to proteins (5 %). Snake venoms contain a large number of biologically active proteins and peptides that are usually similar in structure but not identical to that of prey physiological systems (de Lima et al. 2005; Heise et al. 1995; Tu 1988).

After discovery of "anticancer" activity of snake venom (*Naja* sp.) by Calmette et al. (1933), a number of studies has been carried out on anticancer activity on venom (Gomes et al. 2007; Zhang and Cui 2007; Chiu et al. 2009). Cancer, despite of the all-out efforts from developed countries still causes one in five deaths. Surgery, chemotherapy, and radiotherapy provide inadequate protection and instead affect normal cells along with cancer cells. The search for cancer cure from natural product (plants and animals) has been practiced for over a century and the use of purified chemicals to treat cancer still continues. From the 1940s to 2007, of the 155 new cytotoxic molecules developed, 47 % are actually either natural product or directly derived from them. Several studies have been undertaken during last three decades to establish the anticancer property of venoms and toxins (Gomes et al. 2010). These lead to the discovery of several promising molecule having anticancer activity, some of which are in clinical trial and may emerged to be a future drug in cancer therapy. In our earlier studies, we

T. Bhowmik · P. P. Saha · A. Gomes (✉)
Laboratory of Toxinology & Experimental Pharmacodynamics,
Department of Physiology, University of Calcutta, 92 APC Road,
Kolkata 700009, India
e-mail: agomescu@gmail.com

A. Dasgupta
Department of Biochemistry, University of Calcutta,
35 Ballygunge Circular Road, Ballygunge,
Kolkata 700019, India

have established the anticancer/cytotoxic effect of a lethal protein toxin NK-CT1 present in Indian monocellate cobra, *Naja kaouthia* (Debnath et al. 2010). Recently, Biswas et al. reviewed potential venoms and toxins along with nanoparticle-conjugated venom toxins of snake, amphibians, and bees, etc for possible therapeutic clues against emerging disease (Biswas et al. 2012). The present study reports the increasing efficiencies of anticancer/cytotoxic activity of protein toxin NK-CT1 conjugating with gold nanoparticles.

Present-day nanomedicine exploits carefully a broad variety of structured nanoparticles. These nanoparticles may serve as diagnostic and therapeutic antiviral, antitumor, or anticancer agents (Faraji et al. 2009; Ghosh et al. 2008; Hu and Zhang 2012; Tiwari et al. 2011). The determinant success in therapeutic and diagnostic use of nanoparticle (NP) is the ability to deliver them to desired target. In this sense, NP can be conjugated with biological molecules to make them recognize the biological target. From the point of view of molecular recognition, proteins have a number of properties participating in ligand–receptor and protein–protein molecular interactions. Gold is used for nanoparticle applications because it is unreactive and is not sensitive to air or light. However, gold does like to form bonds with itself and for this reason their surfaces have to be covered with a layer of protective molecules, for example polyethylene glycol (PEG). Capping GNP with PEG could increase stability and biocompatibility. The aim of this work was to explore the conjugation of protein toxin (NKCT1) on GNP surface and characterization of GNP-NKCT1 and their stability. The purpose was to increase the anticancer activity of GNP-NKCT1 from the native protein toxin NKCT1.

2 Materials and methods

2.1 Chemicals

Acrylamide, *bis* acrylamide, Coomassie brilliant blue, 3-(4,5-dimethylthiazol-2-yl)-2,5-diphenyltetrazolium bromide (MTT), sodium dodecyl sulfate (SDS), sodium bicarbonate ($NaHCO_3$), ethidium bromide, RNase A, sodium borohydrate, carboxymethyl (CM) cellulose, propium iodide, acridine orange, trypan blue, hydrogen tetrachloroaurate (III) trihydrate, and de-methoxy sulphoxide (DMSO) were purchased from Sigma-Aldrich Co. (St. Louis, MO, USA). RPMI1640 medium, fetal bovine serum, and penicillium–streptomycin was purchased from Invitrogen (USA). Annexin V-FITC, cell cycle kit, FITC-5-bromo-2′-deoxyuridine (BrdU) kit, and Ki-67 antihuman antibody kits were purchased from BD-Bioscience, USA. All other chemicals were purchased locally and were of analytical grade. Lyophilized *N. kaouthia* crude venom was purchased from Calcutta Snake Park, Kolkata, India.

2.2 Purification of protein toxin NKCT1

NKCT1 protein toxin was purified by ion-exchange column chromatography using CM cellulose and further purified by high-performance liquid chromatography (HPLC; Debnath et al. 2010). The fraction was desalted and concentrated by Centricon (Millipore MWCO 3 k). Purified NKCT1 was checked by SDS-polyacrylamide gel electrophoresis (PAGE) gel electrophoresis method (Laemmli 1970).

2.3 Synthesis of gold nanoparticles and conjugation of NKCT1

The gold nanoparticles were prepared by sodium borohydride reduction method (Samal et al. 2010) with modifications. The synthetic method developed for this experiment consistently produces stable gold nanoparticles provided the conditions are properly controlled. A 25 ml conical was well washed with aqua regia and dried. HAuCl4 (20 mM) and PEG (10 mg/ml) were mixed with sterile phosphate buffer (Liu et al. 2007). Then 100 mM $NaBH_4$ was added dropwise into the conical which was placed on magnetic stirrer at 37 °C for 1 h (pH 7.2). Just after mixing the $NaBH_4$, the color of the reaction mixture was light violet and after several minutes, it changed to deep blue. After 1 h of stirring, mixture is centrifuged at 8,000 rpm for 30 min. Pellet containing large nanoparticles was discarded and 1 mg/ml of protein toxin NKCT1 was added into the supernatant and suspension was kept at room 37 °C for proper conjugation (Table 1).

2.4 Structural characterization of GNP-NKCT1

Conjugation was confirmed by running the 12 % PAGE gel electrophoresis along with low-range molecular marker. CD spectroscopy of the NKCT1 and GNP-NKCT1 was done using Jasco J-815 Circular Dichromism spectrometer with a 0.1-cm cuvette at 25 °C for determination of change in secondary structure of native protein toxin upon its conjugation (Liu et al. 2007; Higuchi et al. 2007).

2.5 Biophysical characterisation of GNP-NKCT1

UV–vis spectroscopy (Perkin Elmer, Lambda-25) measurements from 200 to 700 nm and 400 to 700 nm were performed for NKCT1, GNP-NKCT1, and GNPs only. Spectra were taken at room temperature with 1 cm optical length cuvette with special resolution of 1 nm (Sobczak-Kupiec et al. 2011; Bhattacharya and Srivastava 2003; Olmedo et al. 2008; Sau et al. 2001; Zubarev et al. 2006). Dynamic light scattering measurements were performed in a Malvern Zetasizer Nano ZS apparatus (Malvern Instruments, Milan, Italy) at 25 °C and started 2 min after the cuvette was placed in the dynamic light

Table 1 Three different types gold nanoparticle conjugated NKCT1 and their composition of different chemicals

Type	HAucl$_4$ (20 mM)	PBS (1×)	PEG (10 mg/ml)	NaBH$_4$ (100 mM)	NKCT1 (1 mg/ml)
GNP I	200 μl	8,000 μl	80 μl	40 μl	832 μl
GNP II	240 μl	6,240 μl	62.4 μl	40 μl	1,000 μl
GNP III	360 μl	5,760 μl	57.6 μl	60 μl	612 μl

scattering (DLS) apparatus to allow the temperature to equilibrate. Measurement was carried out 24 h after the preparation of conjugation (Sobczak-Kupiec et al. 2011). The TEM image was obtained on a JEOL JSM 1100 transmission electron microscope. A drop of sample solution was allowed to dry on copper grid overnight (Sau et al. 2001; Zubarev et al. 2006). Atomic force microscope (AFM) image was taken using Atomic Force Microscope (Park System, XE-70, South Korea) in a dark room at 25 °C in noncontact mode for confirmation of nanoparticle and conjugate size (Abdullin et al. 2009).

2.6 Cell culture

Human leukemic lymphoma cell line (U937) and human myelogenous leukemic cell line (K562) were provided by Dr. Aparna Gomes, Scientist, Indian Institute of Chemical Biology, Calcutta, India. Cells were cultured in RPMI 1640 supplemented with 10 % heat-inactivated fetal bovine serum (FBS), NaHCO$_3$ (1.5 g/L), penicillin (100 units), and streptomycin (10 μg/ml). Cells were grown to confluence at 37 °C in a humidified atmosphere of 5 % CO_2 inside an incubator (Heal Force, China).

2.7 Separation and culture of normal lymphocytes

Blood was collected aseptically from the vein of healthy adults (aged 24–30), after informed consent, and transferred to heparinised vial. Lymphocytes were collected from whole blood using Ficoll histopaque after proper dilution with autoclaved saline water (Giri et al. 2006). Then, it was washed with 1× phosphate-buffered saline (PBS) and cultured in sterile complete RPMI 1640 media. Cells were grown in a CO_2 incubator at 37 °C with 5 % CO_2 in humidified condition. The experiment was approved by the institutional human ethical committee (Ref. No. IHEC/AG/HUM/P17/12).

2.8 IC$_{50}$ dose determination of GNP-NKCT1

2.8.1 Cell growth inhibition studies on leukemic cells and normal lymphocytes

U937, K562 (1×10^6) were seeded in 96-well sterile plates and were treated with different concentrations (1–5 μg/ml for U937 cell and 0.5–2 μg/ml for K562 cell of GNP-NKCT1 (I, II, and III)) for 24 and 48 h of incubation. Normal lymphocytes (1×10^6) were also seeded on 96-well and treated with IC$_{50}$ dose of cell lines with respect to standard drug imatinib mesylate (10 μg/ml). The cell growth inhibition studies were done using 0.2 % trypan blue with direct count under light microscope (Olympus, Tokyo) using hemocytometer chamber (Debnath et al. 2010).

2.8.2 Cytotoxicity studies on leukemic cells and normal lymphocytes

Exponentially growing U937 and K562 cells and freshly collected normal lymphocytes at a cell density of 1×10^6/ml were incubated with different concentrations (1–5 μg/ml for U937 cell and 0.5–2 μg/ml for K562 cell IC$_{50}$ dose of both cell line and imatinib mesylate (10 μg/ml for normal lymphocytes)) of GNP-NKCT1 (I, II, and III) for 24 and 48 h at culturable conditions at CO_2 incubator. MTT assay of treated cells were done to confirm its cytotoxic effect (Sargent and Taylor 1989). Of the MTT solution, 40 μl (5 mg/ml) was added 4 h prior to the end of 24 and 48 h of incubation. The formazan granules formed by viable cells were dissolved in DMSO and the absorbance at 570 nm was estimated by measuring with an ELISA reader (BioTek, ELx800).

2.9 Morphological studies for detection of apoptosis

2.9.1 Florescence microscope studies

U937 and K562 cells (1×10^6) treated with IC$_{50}$ dose of GNP-NKCT1 (respective of two cell lines) for 24 h were observed using a fluorescence microscope for morphological changes. The untreated control cells and the GNP-NKCT1-treated cells were harvested separately, washed with PBS, and then stained with acridine orange (100 μg/ml) and ethidium bromide (100 μg/ml, 1:1; Das et al. 2011). The cells were then immediately mounted on slides and observed under fluorescence microscope (Motic Image plus 2.0 software) for determination of the cells undergoing apoptosis.

2.9.2 Confocal microscopic studies

Leukemic cells (1×10^6) were treated with IC$_{50}$ dose of GNP-NKCT1 for 24 h. After 24 h, the untreated control and treated cells were pulled out and washed with ice-cold PBS. The cell

was then stained with 10 μg/ml ethidium bromide and 5 μg/ml of 4′,6-diamidino-2-phenylindole (DAPI), respectively, on ʟ-lysine-coated slide for 5 min (Roy et al. 2008). After mounting on slides, the cells were observed to show the differences in nuclear morphology between the untreated and GNP-NKCT1-treated cells under confocal laser scanning microscope (Leica TCS-SP2 system). Image for ethidium bromide and DAPI were acquired from argon/krypton laser and UV laser line using 590 nm long-pass filter for ethidium bromide, 488 nm long-pass filter for DAPI, and 450 nm bandpass filter for UV images.

2.10 Wound-healing assay

Cells were grown to 99 % confluence in six-well plate at 37 °C of 5 % CO2 incubator. A wound was created by scratching cells in 1.5-cm zone with sterile 200-μl pipette tip after the old medium was washed out. Then, cells were incubated in newly added sterile medium in the absence or presence of GNP-NKCT1 for 24, 48, and 72 h. Cell migration into wound surface was determined under an inverted microscope (Labomed, India).

2.11 Detection of apoptosis by DNA fragmentation and agarose gel electrophoresis

U937 and K562 cells (1×10^6) were treated with IC_{50} dose of GNP-NKCT1 for 24 h. The cells were harvested and washed twice with PBS. The cells were resuspended in 1 ml of digestion buffer (50 mM Tris-HCl, pH 8.0, 10 mM EDTA, and 0.5 % SDS), 100 μg ml^{-1} of proteinase K was added and incubation was done at 65 °C water bath overnight. DNA extraction was done by following the general phenol–chloroform extraction procedure. After centrifugation, the upper layer was mixed with the same volume of isoamyl alcohol. Again after centrifugation, DNA precipitates were washed with 70 % ethanol, dried, and evaporated at room temperature and dissolved in TE buffer (pH 8.0) at 4 °C overnight. To detect DNA fragments, the isolated DNA samples were electrophoresed overnight at 20 V in 1 % agarose gel and stained with ethidium bromide (Roy et al. 2008). DNA fragmentation was observed in UV transilluminator.

2.12 Detection of apoptosis by flow cytometric analysis

In order to investigate the type of cell death induced by GNP-NKCT1, flow cytometric analysis was done by performing dot plot assay (Debnath et al. 2010). The leukemic cells (1×10^6) were treated with IC_{50} dose and 3/4 of IC_{50} dose for 24 h. The cells were pelleted down, centrifuged at 2,000 rpm for 10 min at 4 °C,

and washed with Annexin V-FITC binding buffer (10 mM HEPES, 140 mM Nacl, and 2.5 mM CaCl$_2$, 2H$_2$O; pH 7.4). Again after centrifuging at 2,000 rpm at 4 °C, cell pellets were dissolved in Annexin V-FITC binding buffer containing Annexin V-FITC and propidium iodide. After 15-min incubation in the dark at room temperature, flow cytometric analysis was done. All data were acquired with a Becton-Dickinson FACS Verse double laser cytometer. Flow cytometric reading was taken using 488 nm excitation and bandpass filters of 527/32 nm (for FITC detection) and 585/42 nm (for PI detection).

2.13 Study of cell cycle arrest by flow cytometric analysis

Of the leukemic cells, 1×10^6 were treated with IC_{50} dose and 3/4 of IC_{50} dose of GNP-NKCT1 for 24 h. Cells were washed with PBS, fixed with ice-cold 70 % ethanol which was added drop-wise in stirring condition on Vortex, and kept at −20 °C overnight. Cells were pelleted down, washed twice with cold PBS, and finally dissolved in PBS treated with RNase A for 30 min at 37 °C and stained with propium iodide (20 μl from 50 μg/ml) and kept in the dark for 15 min. Cell cycle phase distribution of nuclear DNA was determined on FACS, fluorescence detector equipped with 488 nm laser light source and 623 nm bandpass filter (Hosta et al. 2009; Lin et al. 2006).

2.14 Estimation of total DNA by Ki-67 antihuman antibody using FACS

U937 and k562 cells (1×10^6) were treated with IC50 dose and 3/4 of IC_{50} dose of GNP-NKCT1 for 24 h. Cells were washed with PBS and fixed with ice-cold 70 % ethanol and kept at −20 °C overnight. Cells were washed with buffer (PBS with 1 % FBS, 0.09 % NaN3 pH 7.2) twice and the cells were resuspended in PBS. Of the Ki-67 antibody cell, 20 μl/100 μl were added (Ross et al. 2003). After mixing gently, it was kept for 20 min at room temperature in the dark. After centrifugation at 1,000 rpm for 5 min, 500 μl of PBS was dissolved and added to 10 μl (50 μg/ml) of PI staining solution and incubated for 15 min at room temperature in the dark. Then, the sample was analyzed with FACS verse (BD Bioscience).

2.15 Estimation of replication cycle by BrdU incorporation using FACS

Exponentially growing U937 and k562 cells (1×10^6) were cultured on RPMI medium containing 10 μl BrdU (10 μg/ml; Jayat and Ratinaud 1993; Holm et al. 1998). After 1 h, cells were treated with IC_{50} dose and 3/4 of IC_{50} dose of GNP-NKCT1 and kept at CO$_2$ incubator for 24 h.
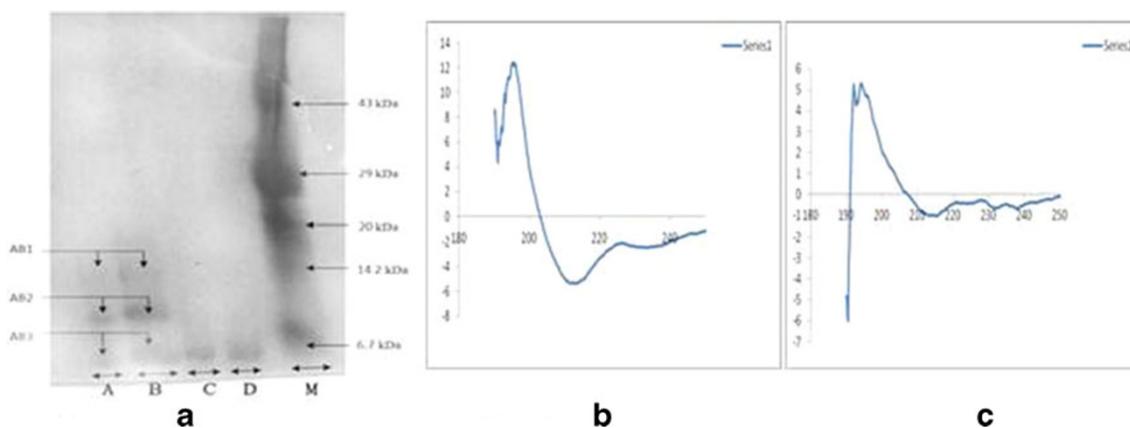
Fig. 1 PAGE of conjugated sample. *M* marker, *A* and *B* GNP-NKCT1, and *C* and *D* native NKCT1. Two types of conjugate were held (AB1, 14 kDa; AB2, 10 kDa). AB3 represents free protein (4–5 %) in conjugated solution (**a**). CD spectra of secondary structure of NKCT1 upon its conjugation with GNP. **b** Graph presents the secondary structure of NKCT1 (23 % α helix, 19 % β sheet, and 35 % random coil). **c** Graph presents the secondary structure of GNP-NKCT1 (43.5 % α helix, 24.5 % β sheet and 32 % β turn)

Cells were washed with PBS and fixed with permealization buffer for 20 min. After washing again with PBS, Dnase (5 μg/ml) was added and incubated for 1 h at 37 °C. Anti-BrdU antibody was added to it and kept in the dark for 20 min after PBS washing. Incubated with 7-ADD for 15 min at dark condition, the sample was analyzed with

Fig. 2 Surface plasmon resonance spectroscopy of NKCT1 (λ_{max}=220 nm) (**c**), GNP (λ_{max}=530 nm) (**a**) and GNP-NKCT1 (both the λ_{max}=220 nm and λ_{max}= 528 nm) (**b**) detected by UV–Vis. Hydrodynamic diameter of GNP and GNP-NKCT1 were showed by DLS. The size of only GNP was 2–8 nm with average size of 4 nm (**d**) and GNP-NKCT1 conjugate particle showed 68–122 nm with average of 92 nm (**e**)
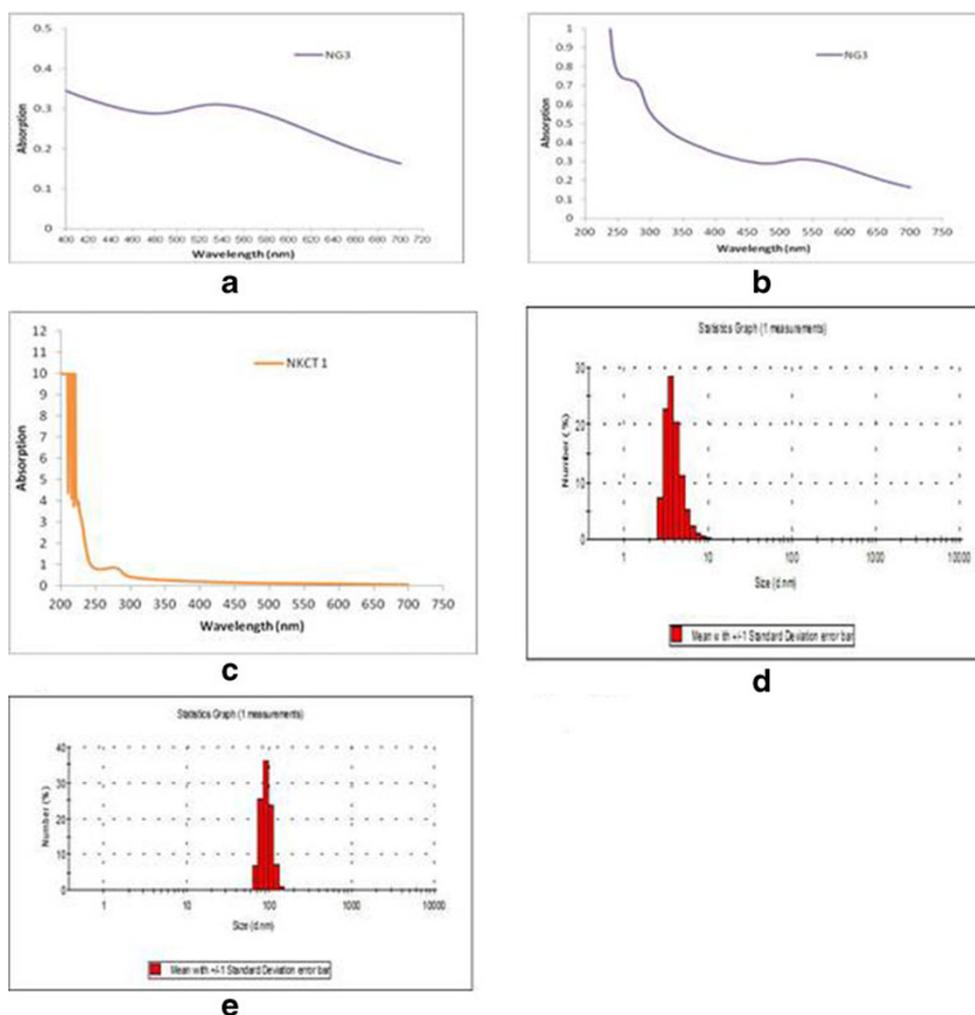
Fig. 3 Transmission electron microscopy (TEM) photograph of goldnanoparticle (*bar* 50 nm). Only GNP (**a**) and GNP with protein core (**b**). *Arrow* indicates protein core around the GNP. Actual size of gold nanoparticle measured by atomic force microscope. Where only GNP showed 5–25 nm (**c**), GNP-NKCT1 showed 40–220 nm (**d**)
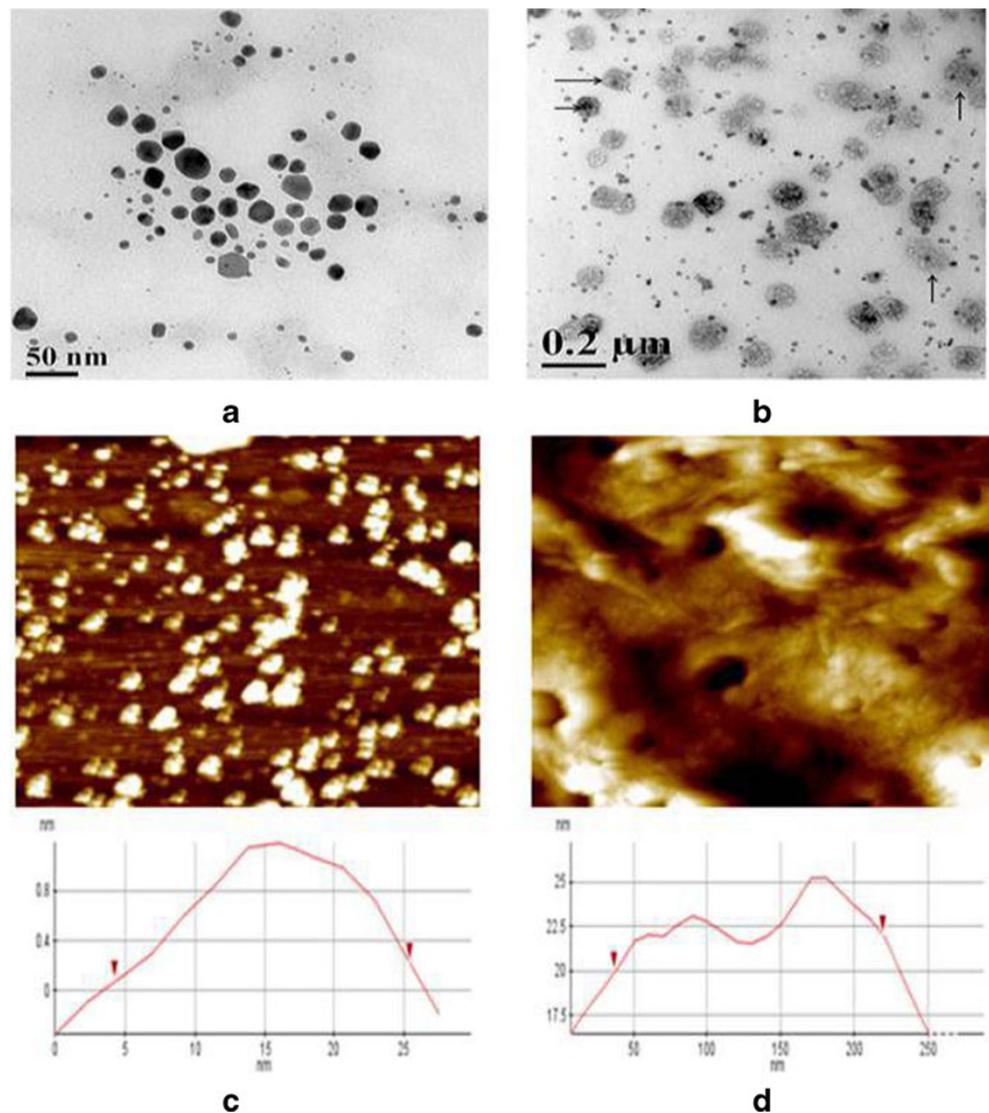
FACS verse using 507 nm long-pass filter, 527/32 bandpass detector, and 488 nm laser light source.

2.16 Statistical analysis

All values are represented as arithmetic mean±SEM. Statistical analysis was done by Student's *t* test. A probability value of less than 0.05 was chosen as the criterion of statistical significance.

3 Results

3.1 Purification of NKCT1

As previously reported by Debnath et al., NKCT1 was purified by ion-exchange method and 3.24 mg/ml protein was estimated by Lowry's method (Lowry et al. 1951).

HPLC showed only a single peak with a retention time of 10 min. SDS-PAGE showed single band with molecular weight of 6.7 kDa (Fig. 1a).

3.2 Conjugation of GNP with protein toxin NKCT1

Polyacrylamide gel electrophoresis of GNP-NKCT1 showed two bands as compared with the single band of NK-CT1. Molecular weight of the two bands of GNP-NKCT1 was found to be 10 and 14 kD, respectively (Fig. 1a), unconjugated NK-CT1 (above 4–5 %) was present and produced faint band in PAGE. CD spectra showed, native NK-CT1 contained 23 % α-helix, 19 % β-sheet, and 35 % random coil and GNP-NKCT1 contained 43.5 % α-helix, 24. 5 % β-sheet, and 32 % β-turn. Percent change after conjugation was found to be 20.5 % of α-helix, 5.5 % β-sheet. Found in the secondary structure of GNP-NKCT1, 32 % of β-turn
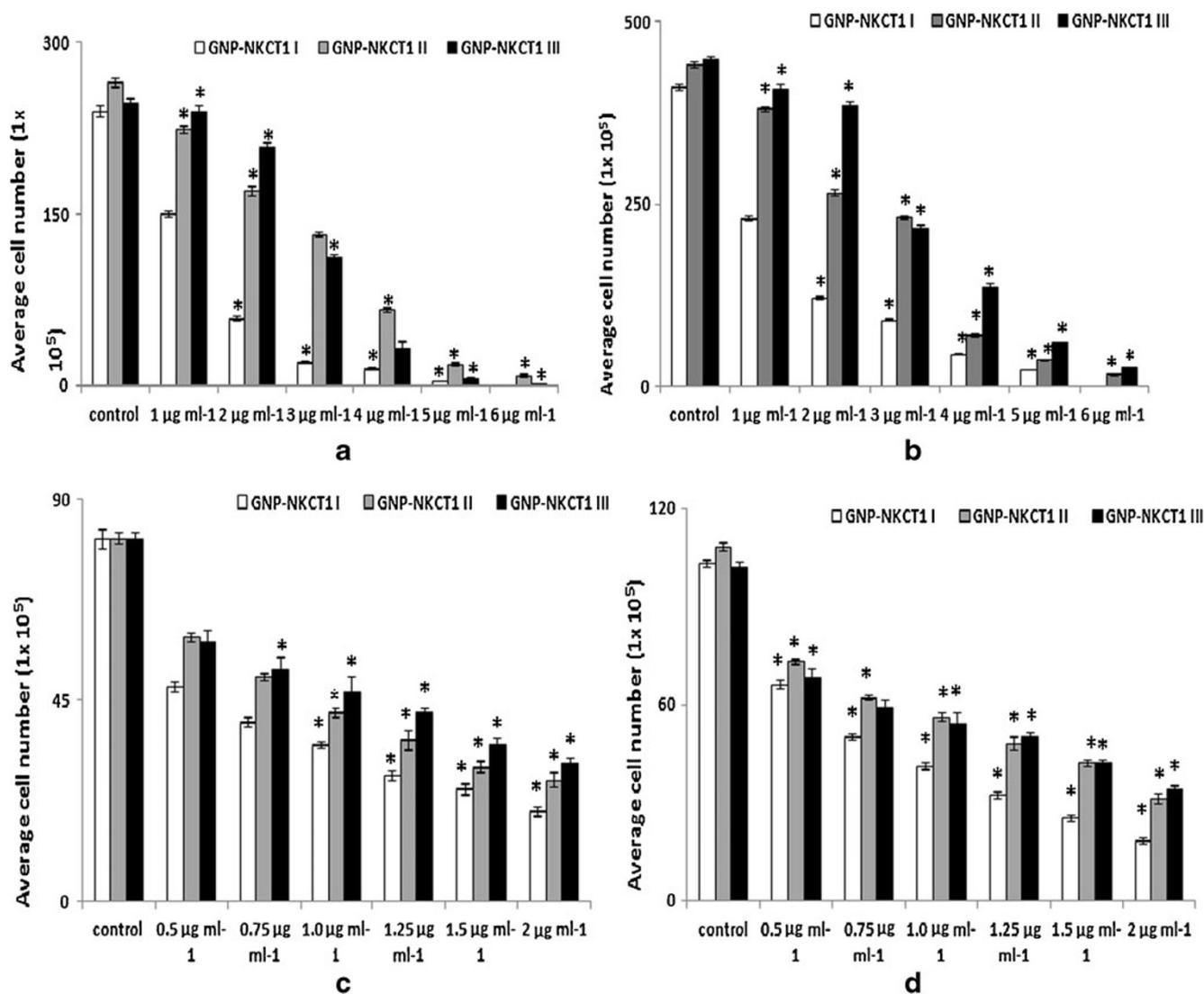
Fig. 4 Bar diagram presents the IC$_{50}$ dose of GNP-NKCT1 (*1*, *2*, and *3*) on U937 cell line (**a** and **b**) and K562 cell line (**c** and **d**), determined by trypan blue exclusion method. On U937 cell after 24 h IC$_{50}$ dose=1.5 μg/ml (**a**) and after 48 h IC$_{50}$ dose=1.2 μg/ml (**b**). On K562 cell after 24 h. IC$_{50}$ dose=0.8 μg/ml (**c**) and after 48 h IC$_{50}$ dose=0.75 μg/ml (**d**). Result of MTT assay on U937 cell line [**e** (24 h) and **f** (48 h)] and on K562 cell [**g** (24 h) and **h** (48 h)]. Effect of GNP-N KCT1 and imatinib mesylate on normal lymphocyte. Cell count by trypan blue exclusion (4i) and by MTT assays (4j). Each value represents quadruplicate samples of mean±SEM. *P<0.05 as compared to control

was found in the secondary structure of GNP-NKCT1 as compared with the 35 % random coil of NK-CT1. This data confirmed that cysteine/amide residue (Dolati et al. 2011) of the amino acid chain was conjugated with gold nanoparticle directly with the surface or via PEG attached with the GNP surface (Fig. 1b and c).

3.3 Biophysical characterization of GNP-NKCT1

The gold nanoparticle formed was light violet/pink color having plasmon resonance at 530 nm (Fig. 2a). The plasmon resonance of GNP-NKCT1 was formed at the 528 and

220 nm, as compared with the plasmon resonance of NKCT1 which was at 220 nm (Fig. 2b and c). The hydrodynamic diameter of the nanoparticle measurement with DLS was found in the range of 2–8 nm, with an average size of 4 nm (Fig. 2d). GNP-NKCT1 diameter was 68–122 nm, with an average size of 92 nm (Fig. 2e). Figure 3 shows high-resolution TEM micrograph (HR-TEM) of bare GNP and NKCT1-coated GNP (Fig. 3a, b). The presence of layer around the nanoparticle core was due to NKCT1, which was observed by uranyl acetate staining. As observed, the PEG and one/two protein molecule covered the whole surface of the nanoparticle and increased the hydrodynamic size
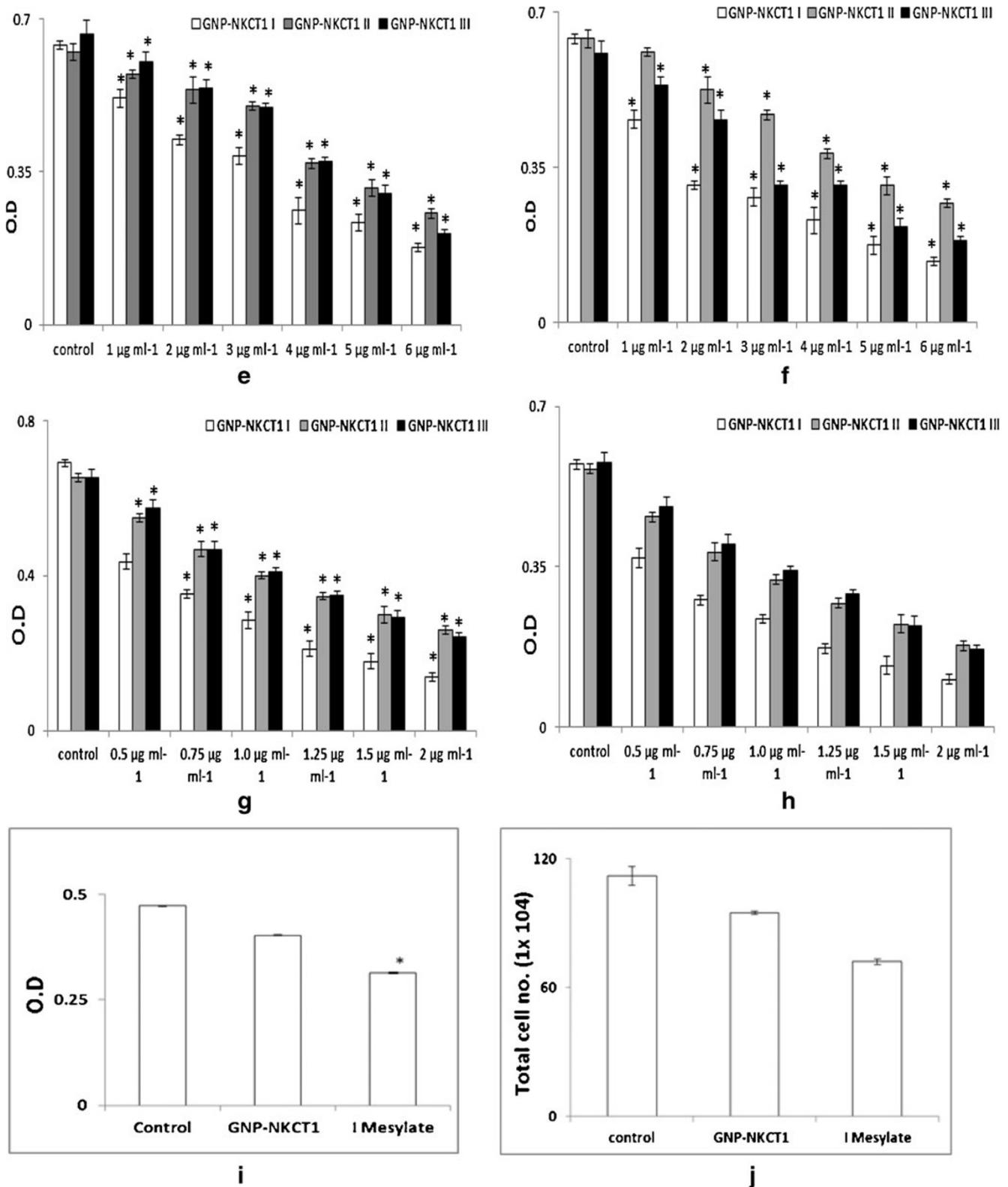
Fig. 4 (continued)

of NKCT1-capped gold nanoparticle. AFM showed the cluster of the gold nanoparticle size and it was found to be 4–25 nm whereas with protein core, it was 45–225 nm (Fig. 3c, d).

Table 2 IC_{50} dose of GNP conjugated NKCT1 on leukemic cell lines

Cell line	GNP type	IC50 (µg/ml) of conjugated GNP-NKCT1	
		24 h	48 h
U937	GNP-NKCT1-III	1.60±0.09	1.20±0.05
	GNP-NKCT1-II	3.80±0.10	3.00±0.12
	GNP-NKCT1-I	3.40±0.08	2.80±0.10
K562	GNP-NKCT1-III	0.80±0.07	0.75±0.03
	GNP-NKCT1-II	1.10±0.06	1.00±0.05
	GNP-NKCT1-I	1.25±0.07	1.20±0.01

3.4 Cell growth inhibition study and cytotoxicity study

GNP-NKCT1 at concentrations of 1–5 µg/ml (U937 cell line) and 0.5–2 µg/ml (K562 cell line) significantly inhibited the growth of the respective leukemic cells compared with the control cell and normal lymphocyte cell in a time- and concentration-dependent manner. Cell count (Fig. 4a–d) and MTT assay (Fig. 4e–h) revealed that IC_{50} value for U937 and K562 cells were 1.2 and 0.75 µg/ml of GNP-NKCT1-I only. When normal human lymphocytes were treated with GNP-NKCT1 (1.2 µg/ml) for 48 h, there was 15–16 % decrease in count as compared to untreated control (Fig. 4i–j). But when normal human lymphocyte were treated with standard drug imatinib mesylate (10 µg/ml) for 24 h, there was 34–35 % decrease in count (Fig. 4i–j). This showed that cell death after GNP-NKCT1 treatment was significantly less in case of normal lymphocytes as compared to treated leukemic cells and also in comparison to the standard imatinib mesylate, toxicity of GNP-NKCT1 towards normal cells is less. The other two conjugated product, GNP-NKCT1 (1) and GNP-NKCT1 (2) did not show promising result. In U937 cells, IC_{50} dose were 3.0 and 2.8 µg/ml, respectively, for GNP-NKCT1-II and GNP-NKCT1-III, whereas in K562 cells IC_{50} dose were 1 µg/ml and more than 1 µg/ml, respectively, for GNP-NKCT1-II and GNP-NKCT1-III (Table 2). As GNP-NKCT1-I showed very promising result, it was selected as an experimental sample for rest of the experiment and it was abbreviated GNP-NKCT1 only.

3.5 Morphological studies for detection of apoptosis

Morphological observations of treated cells from both the cell lines under fluorescent microscope showed intact nuclei in control cell that gave bright green fluorescence (Fig. 5a and c) whereas treated cells showed intense orange–red fluorescence showing signs of apoptosis (Fig. 5b and d). Confocal microscopes revealed chromatin disintegration and formation of apoptotic bodies (Fig. 5e, g, i, and k) whereas control cell showed intact cell (Fig. 5f, h, j, and l).

3.6 GNP-NKCT1 inhibited leukemic cell migration

As shown in Fig. 6, the cell migration was obviously inhibited by GNP-NKCT1 with time-dependent manner. Where control cell (absence of GNP-NKCT1) showed growth in wound zone within 24 h, the treated cell showed very little growth in scratching zone after 48 h. After 72 h, 95.80 % control U937 cells migrated in the wound zone but it was only 40. 88 % in treated U937 cell; in case of K562 cells where in 99. 10 % were filled, only 51.60 % were filled by treated cell.

3.7 Detection of apoptosis by DNA fragmentation and agarose gel electrophoresis

The gel pattern of DNA samples isolated from untreated control cell lines showed intact bands whereas the gel pattern of DNA samples isolated from GNP-NKCT1-treated U937 (Fig. 7a) and K562 cells (Fig. 7b) showed smeary band. So, the observations confirmed that the treatment with GNP-NKCT1 causes apoptosis in human leukemic cells.

3.8 Detection of apoptosis by flow cytometric analysis

In the flow cytometric analysis, lower left (LL) quadrant (Annexin V–/PI–) is regarded as population of live cells, lower right quadrant (LR; Annexin V+/PI−) is considered as the cell population at early apoptotic stage, upper right quadrant (UR; Annexin V+/PI+) represents the cell population at late apoptotic stage and upper left quadrant (Annexin V−/PI+) is considered as necrotic cell population. Flow cytometric data analysis revealed that after 24 h of treatment of GNP-NKCT1 (IC_{50} dose) 0.37 % in LL quadrant, 57.16 % in LR quadrant, and 42.47 % in UR quadrant of U937 cells (Fig. 8b) with respect to 98.51 % in LL quadrant, 0.17 % in LR quadrant, and 0.45 % in UR quadrant of control cell (Fig. 8a) and 22.27 % in LL quadrant, 75.89 % in LR quadrant, and 1.81 % in UR quadrant of K562 cells (Fig. 8d) with respect to 96.37 % in LL quadrant, 2.95%in LR quadrant, and 0.55 % in UR quadrant of control cell (Fig. 8c).

3.9 Study of cell cycle arrest by flow cytometric analysis

The flow cytometric analysis showed that when compared with that of the untreated control U937 cells and K562 cells, 24 h of GNP-NKCT1 (3/4 of IC_{50} dose) treatment caused a progressive increase in the number of cells with 2N DNA content, indicating that the GNP-NKCT1 treatment inhibited the growth of U937 and k562 cells by cell cycle arrest in G1 phase. Where U937-treated cell showed 78.58 % G1+G0, 6. 84 % S, and 8.81 % G2+M (Fig. 8f), the control cell showed 48.88 % G1+G0, 40.80 % S, and 8.98 % G2+M (Fig. 8e) where k562 cells showed 62.47 % G1+G0, 31.62 % S, and 2. 98 % G2+ M (Fig. 8h), the control cell showed 35.84% G1+ G0, 50.03 % S, and 11.86 % G2+M (Fig. 8g).
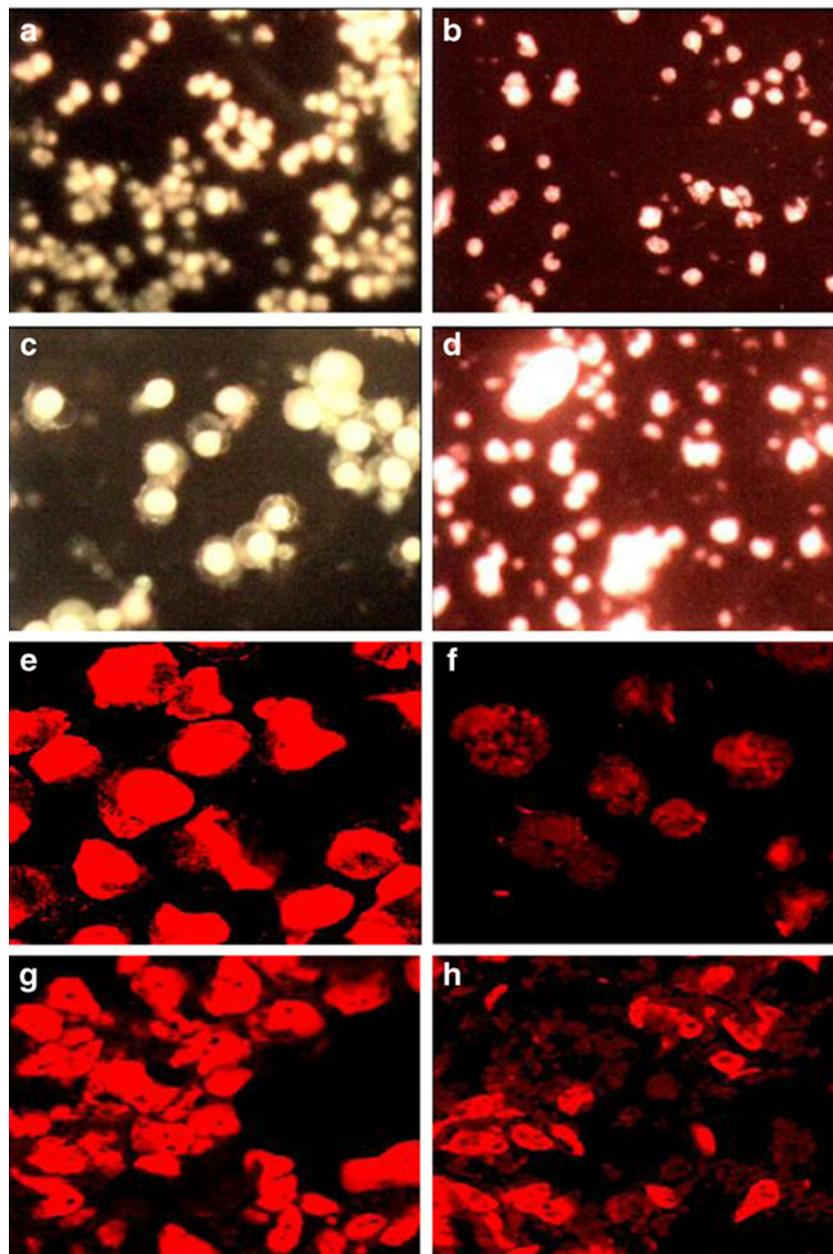
Fig. 5 Fluorescence microscopic images of control U937 (**a**), K562 (**c**), GNP-NKCT1 treated U937 (**b**), treated K562 (**d**) cell line. The control cells gave bright green fluorescence for their intact nuclei whereas both treated cell line red fluorescence showing signs of apoptosis. Confocal microscopic images of control U937 (**e** and **i**), K562 (**g** and **k**) and GNP-NKCT1 treated U937 (**f** and **j**), treated K562 (**h** and **l**) cell lines. The treated cells indicated apoptotic changes like nuclear disintegration, membrane disruption. **e**–**h** Cells stained with propium iodide and **i** to **l** are cells stained with DAPI

3.10 Estimation of total DNA by Ki-67 antihuman antibody using FACS

The flow cytometer detected, DNA content of control cells was much higher than the treated cell lines. In case of control, U937 cell showed 97.06 % dividing phase and control K562 cell showed 88.70 % (Fig. 9a and c), but in treated cell line dividing cell were 46.11 and 65.68 %, respectively (Fig. 9b and d). This result proved that control cell showed more dividing phase (S phase and G2+M phase) than treated cell line.

3.11 Estimation of replication cycle by BrdU incorporation using FACS

The immunofluorescent staining of incorporated bromodeoxy uridine (BrdU) and flow cytometry analysis provide a high-resolution technique to determine the frequency and nature of
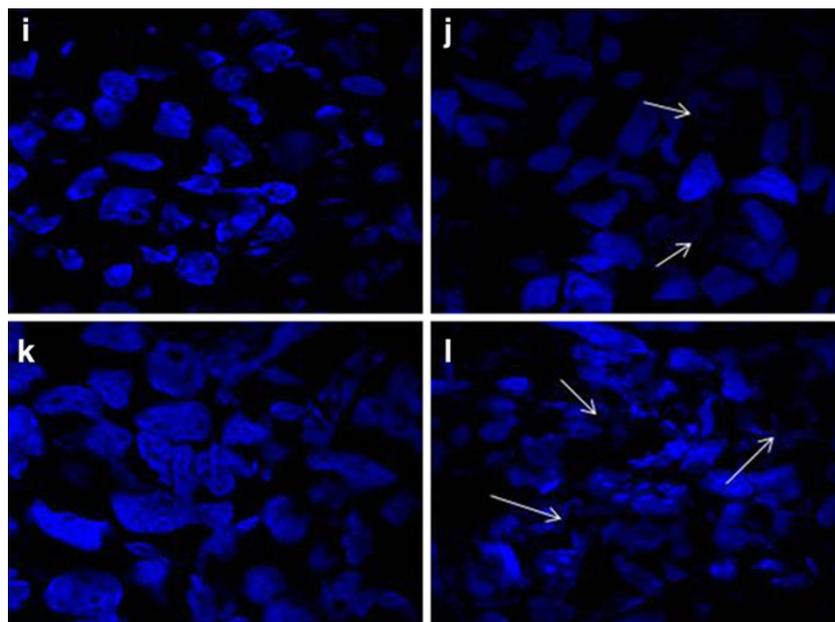
Fig. 5 (continued)

individual cells that have synthesized DNA. In this method, BrdU (an analog of DNA precursor thymidine) is incorporated into newly synthesized DNA by cells entering and progressing through the S (DNA synthesis) phase of cell cycle. Often, staining with a dye that binds to total DNA such as 7-ADD is coupled with immunofluorescent BrdU staining. With this combination, two-color combination and two-color flow cytometry analysis permits the enumeration and characterization of cells that are actively synthesizing DNA in terms of their cell cycle position. BrdU incorporation via replication cycle (synthesis phase) was significantly decreased in GNP-NKCT1 treated cell with respect to control cell. Control U937 cell showed 54.04 % synthesis phase and GNP-NKCT1 treated cell showed 20.44 % (Fig. 9e and f). In other set of experiment, GNP-NKCT1 treated K562 cell showed 50.7 % BrdU incorporation with respect to 71.04 % of BrdU in control K562 (Fig. 9g and h).

4 Discussions

The number of natural product-derived drugs present in the total drug launches from 1940 to 2011 was recently analyzed and it was concluded that natural products are still a significant source of new chemotherapeutic agent, especially anticancer (Newman et al. 2003). Although many chemotherapeutic drugs are used clinically, the overall survival of leukemia patients is far from satisfactory. Recent advances in nanotechnology have stimulated different applications in biomedicine where nanoparticles are used as drug delivery vehicles allowing rational manipulation of pharmacological profiles

of drugs encapsulated in them and hence their concomitant therapeutic indices(Wang et al. 2009). The present investigation confirmed the increase of percentage of cytotoxicity activity and apoptosis against two human leukemic cell lines U937 and K562 including the conjugation of protein toxin NKCT1 with gold nanoparticle. Gold nanoparticle has special attraction to sulfur bond (Fan et al. 2003). Though protein toxin NKCT1 has cysteine residue, we used PEG for more stability of GNP-NKCT1. CD spectra showed the change in secondary structure that might be the bonding of N-terminal NH_2 or internal amide group of NKCT1 via the hydroxyl (OH) group of PEG with gold nanoparticle; still some work (i.e., FTIR, XPS, EELS) should be done to investigate the proper bonding of GNP with NKCT1 (Liu et al. 2007; Shi et al. 2004). UV–vis spectroscopy showed surface plasmon resonance at 520–540 nm which is the primary characteristics of gold nanoparticle formation (Triulzi et al. 2008). For using of strong reducing agent like sodium borohydrate for the preparation of GNP, it became very much polydisperse in size. The formation of GNPs by $NaBH_4$ and sodium citrate method was different. In sodium citrate method, after formation of GNPs, it became capped by citrate ion that is why they repelled each other and stayed single in solution. But in $NaBH_4$ method, they became as Au 0 state that is why they attracted each other and formed the cluster of GNPs with time-dependent manner. Where HR-TEM confirmed the formation of various size of gold nanoparticle formation, PAGE gel electrophoresis showed molecular weight became 10 to 14 kDa which means one or two protein chains were conjugated per gold nanoparticle. The GNP-NKCT1 is stable at room temperature and showed the same efficiency effect after 1 month of storing at

Fig. 6 Migration of both cell lines was affected by GNP-NKCT1. Only 40.88 and 51.60 % cells were recovered after scratching in U937 and K562 cell line, respectively. All the value represents quadruplicate samples of mean±SEM. *P<0.05 as compared to control
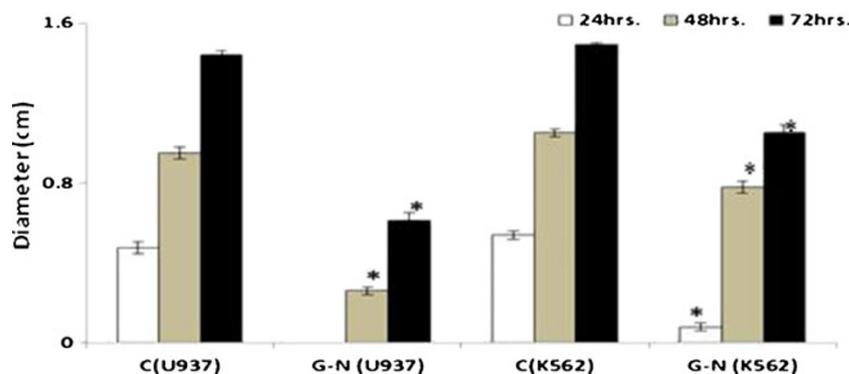
room temperature (30°±5 °C); GNP not only increases the life span of NKCT1. Our study emphasize on the already established fact that GNP-NKCT1 were taken up more by leukemic cell in comparison to native protein NKCT1. The lower uptake of native NKCT1 is attributed to the resistance experienced by them due to P-gp pump highly expressed on leukemia cells (Hui et al. 2008) which acts as an energy drug efflux pump and leads to decrease in cytotoxic protein accumulation. The nanoparticle conjugation system escapes the P-gp pump as their uptake is mediated by specific endocytic processes (Sahoo and Labhasetwar 2005). Thus, gold nanoparticle-conjugated NKCT1 preferentially delivered into the cells or subcellular organelle like mitochondria or lysosome for eliciting a better therapeutic effect than native protein NKCT1. The antiproliferative and the cytotoxic activities of GNP-NKCT1 were supported by observations in cell growth inhibition studies and in MTT assays, respectively. GNP-NKCT1 inhibited the growth and electron transport chain

via blocking of succinate dehydrogenase in mitochondria of U937 and K562 cells in concentration- and time-dependent manner. In separate study, we saw GNP-NKCT1 possesses potent immunomodulatory activity and that concentrations (IC$_{50}$ dose of U937 cell) showed very less toxic effect on normal lymphocyte cell line as observed by trypan blue exclusion and MTT assay. This finding reveals that GNP-NKCT1 preferentially acts on leukemic cells. Competency of drug-loaded nanoparticles in inhibiting the growth of K562 cells were recently studied by Palma et al., where imatinib-loaded microcapsules were used to targeted leukemia stem cells more profoundly than native imatinib (Palma et al. 2010). Similar approach was also taken up by Luo et al. and Yang et al. who have used *N* succinyl chitosan nanoparticles and lipid nanoparticles on K562 cells for better antitumor effect (Luo et al. 2009; Yang et al. 2009).

There are two main strategies by which chemotherapeutic agents are capable of exerting their effect: (1) is by induction of apoptosis and (2) is by cell cycle inhibition. Many of the compounds under study as antitumor agents act at multiple steps in cell cycle, and their effects may be cytostatic or cytotoxic, depending on the cell cycle status of the target cells (Shapiro and Harper 1999). In this context, our study indicated that at lower concentration (0.5 μg/ml for K562 cell line and 0.9 μg/ml for U937 cell line) of GNP-NKCT1 was able to cause cell cycle arrest at particular phase while at a higher concentration (0.75 μg/ml for K562 cell line and 1.2 μg/ml for U937 cell line) it was capable of inducing apoptosis. Central dogma of the cell was inhibited by the treatment of GNP-NKCT1. BrdU, which is the analog of the DNA precursor thymidine, is incorporated during the first major round of cell cycle activity. Flow cytometry detected inhibition of replication as treated
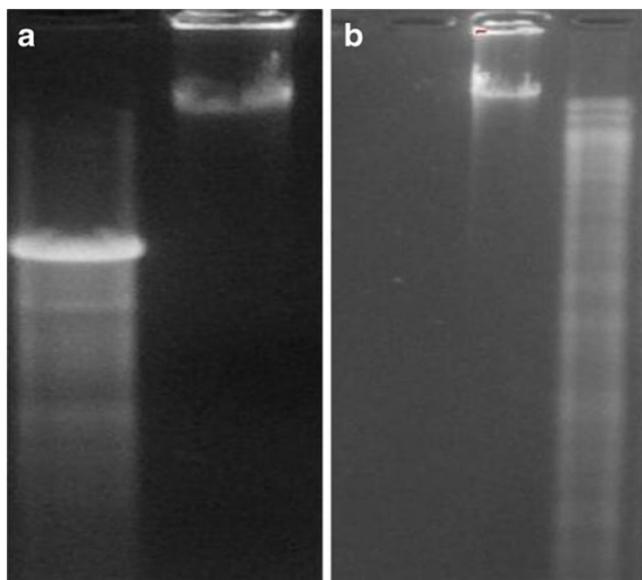
Fig. 7 The gel pattern of DNA samples isolated from **a** control U937 cells (*2*), treated U937 cells (*1*), **b** control K562 cells (*1*) and treated K562 cells (*2*). Treated with GNP-NKCT1 showed smeary band of DNA in both cell lines indicating the process of apoptosis

Fig. 8 Flow cytometry analysis of U937 and K562 cells stained with ▶ Annexin V-FITC-PI, after treatment with NK-CT1. Control U937 cells (**a**), treated U937 cells (**b**), control K562 cells (**c**), and GNP-NKCT1 treated K562 (**d**). Flow cytometry analysis of cell cycle of untreated control U937 cells (**e**), GNP-NKCT1-treated U937 (**f**), control K562 cells (**g**), and treated K562 cells (**h**). Histogram of both the treated cell line showed the arrest of cell cycle in G1 phase (*x*-axis denotes fluorescence intensity of propium iodide and *y*-axis denotes cell count)
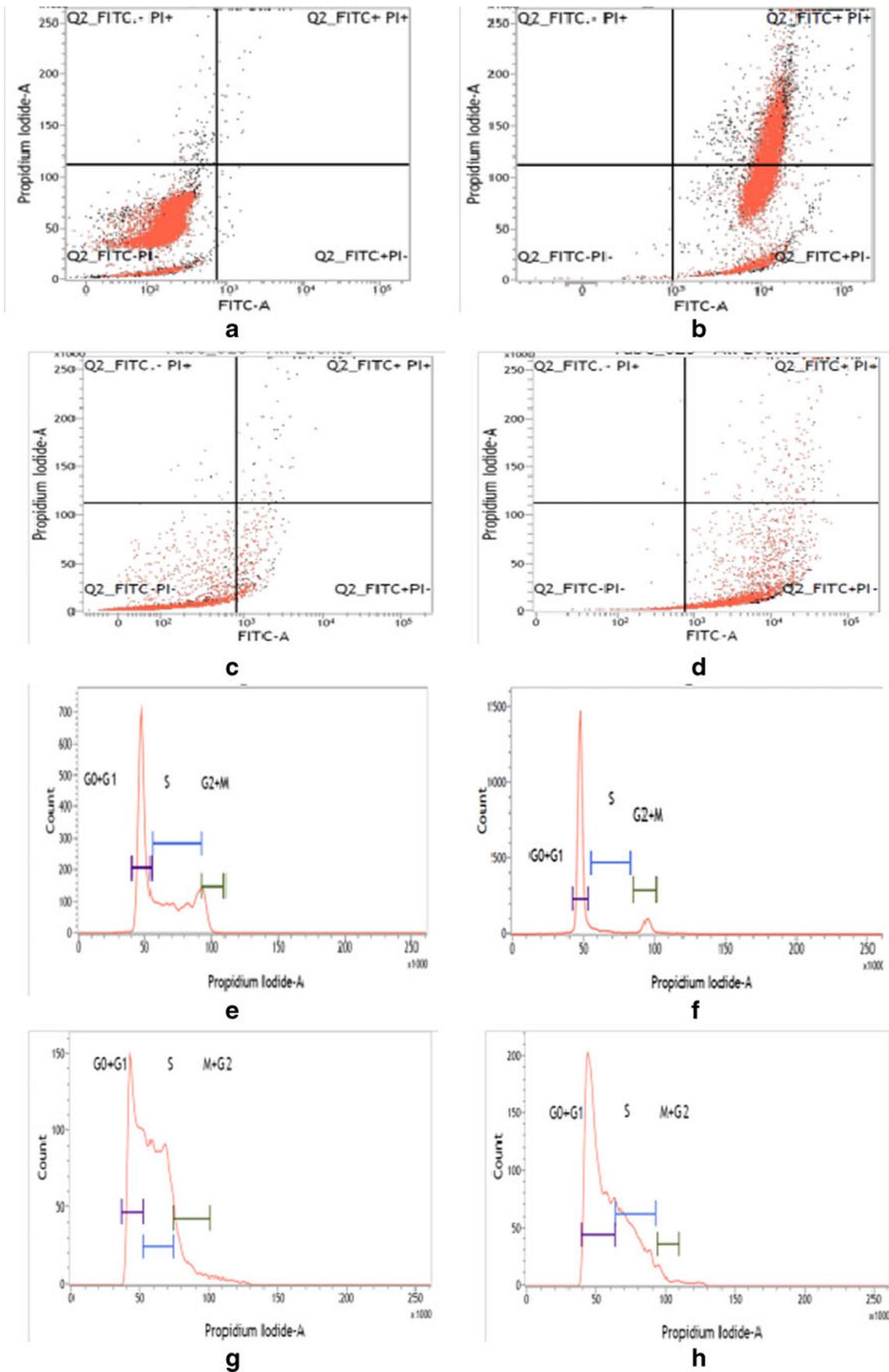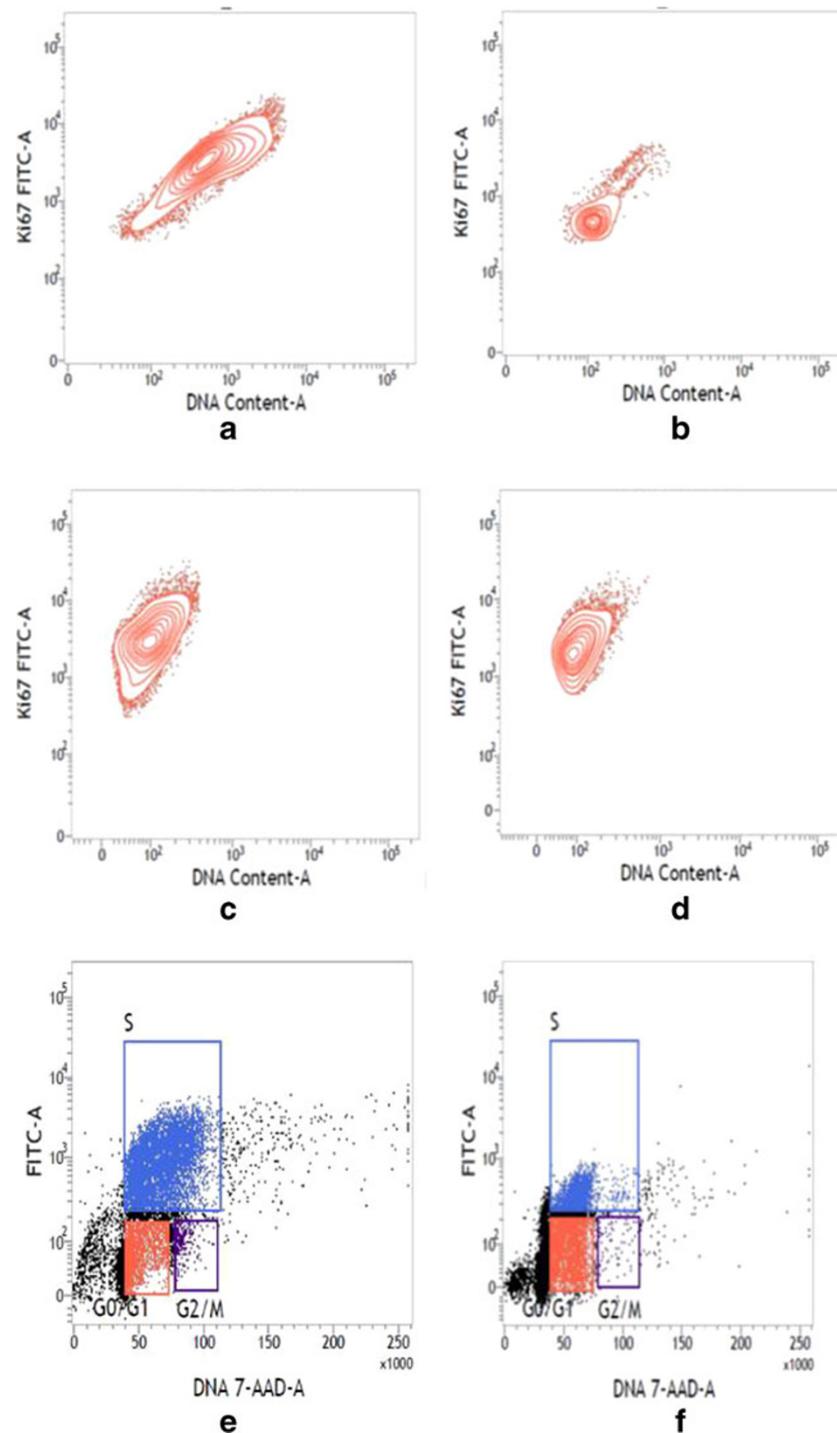
Fig. 9 Flow cytometry analysis of DNA content of control U937 (**a**), treated U937 (**b**), control K562 (**c**), and treated K562 (**d**) cells. Contour plot of both treated cell line showed less number of nuclear proliferation-associated protein (*x-axis* DNA content and *y-axis* fluorescence intensity of FITC). Flow cytometry analysis of replication cycle of control U937

(**e**), GNP-NKCT1 treated U937 (**f**), control K562 (**g**), and GNP-NKCT1 treated K562 (**h**) cell lines. Control cells showed more BrdU incorporation by indicating more synthesis phase, whereas treated cell line showed less BrdU incorporation indication less synthesis phase and signs of cell cycle arrest

cell showed less BrdU signal in synthesis phase. Similar work was done by Ghiringhelli et al. where they measured the incorporation of BrdU into T reg cells residing in tumor beds and lymphoid organs of TFM versus tumor-bearing mice

(Ghiringhelli et al. 2005). Protein expression on the nuclear surface became less as detected by ki-67, a nuclear proliferation associated antigen expressed in all active stages of the cell. After GNP-NKCT1 treatment, cell cycle arrest as well as
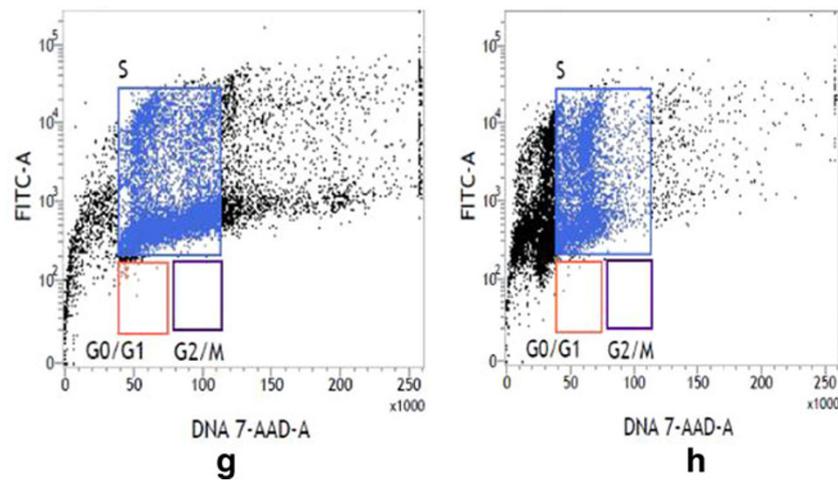
Fig. 9 (continued)

programmed cell death occurred via apoptosis and for this reason migration of cell became very less after wound healing.

Apoptosis is an important continuous and highly regulated cellular process resulting in destruction of undesirable cells during development or homeostasis in multicellular organisms (Kaufmann and Hengartner 2011). Apoptogenic activity of GNP-NKCT1 was investigated by different morphological studies like fluorescence microscopic, confocal microscopic, and phosphatidylserine externalization studies. The process of apoptosis is characterized by several morphological changes such as membrane blebbing, chromatin condensation, and nuclear fragmentation. Fluorescence microscopic image clearly showed nuclear disintegration of GNP-NKCT1-treated leukemic cells compared with control cell when stained with acridine orange and ethidium bromide. The control cells showed bright green fluorescence as the live cells with intact membrane excluded ethidium bromide and only acridine orange could enter into them. On the contrary, GNP-NKCT1-treated cells showed more intense red fluorescence and reduced green fluorescence since apoptotic and necrotic cells could not exclude the dyes and gave a combination of orange–red fluorescence. Apoptogenic activity of GNP-NKCT1 was further evidenced from the confocal microscopy images of treated leukemic cells when compared to control cell. After GNP-NKCT1, leukemic cell lines showed several signs of apoptosis like chromatin condensation and nuclear fragmentation whereas the untreated control cells were with intact nuclei. Externalization of PS from inner leaflet to outer leaflet of the membrane is the hallmark of apoptosis. Externally translocated PS bind with Annexin V in a calcium-dependent manner. Flow cytometry detected Annexin V-FITC and showed the dot plot supporting the fact that treatment with GNP-NKCT1-induced apoptosis in the leukemic cells. Cells undergoing apoptosis usually exhibited fragmentation of the cell into membrane-bound apoptotic bodies, nuclear and cytoplasmic condensation, and endolytic cleavage of the DNA into small oligonucleosomal

fragments (Thatte et al. 2000). Further evidence in support of apoptogenic activity of GNP-NKCT1 was obtained from gel patterns of agarose gel electrophoresis. GNP-NKCT1 showed smeary bands, a typical indication of apoptosis whereas the untreated control cells showed intact DNA bands. Apoptosis is a tightly regulated process, which involves changes in expression of distinct set of genes. Two of the major genes responsible for regulating the mitochondrial apoptosis pathway are antiapoptic Bcl-2 and proapoptic bax (Tong et al. 2004). Debnath et al. reported that NKCT1-induced the apoptosis in leukemic cell line like U937 and K562 via activation of Bcl2: bax and cleaved PRAP levels with increasing dose of NKCT1. We also believed that our conjugated GNP-NKCT1 follow the same signaling pathway. Further work is going on molecular signaling.

5 Conclusion

This study exhibited that conjugation of gold nanoparticle with NKCT1 work in synergistic manner lowering both dose of administration and time of action of the NKCT1 ensuring that GNP release the NKCT1 to the target cell by controlled manner and two- to threefold increase the cytotoxic effect while minimizing the toxic effect of NKCT1. This conjugation was capable of showing high antileukemic activity by inducing cell cycle arrest and promoting apoptosis regulating activities like nuclear fragmentation. Moreover, regulation of various biochemical pathways after inhibiting the transcriptional and translational level by GNP-NKCT1 treatment supports the evolving concept that such nanoparticle conjugation may be helpful for leukemia therapy in the near future.

References

Abdullin IT, Bondar OV, Nikitina II, Bulatov ER, Morozov VM, Hilmutdinov KA, Salakhov KM, Culha M (2009) Effect of size and protein environment on electrochemical properties of gold nanoparticles on carbon electrodes. Bioelectrochemistry 77:37–42

Bhattacharya S, Srivastava A (2003) Synthesis of gold nanoparticles stabilised by metal-chelator and the controlled formation of close-packed aggregates by them. Proc Indian Aacd Sci Chem Sci 115:613–619

Biswas A, Gomes A, Sengupta J, Datta P, Singha S, Dasgupta AK et al (2012) Nanoparticle-conjugated animal venom toxins and their possible therapeutic potential. J Venom Res 3:15–21

Calmette A, Saenz A, Costil L (1933) Effects du venin de cobra sur les greffes cancereuses et sur le cancer spontane (adenocarcinoma) de la souris. C R Acad Sci 197:205–209

Chiu CC, Lin KL, Chien CM, Chang LS, Lin SR (2009) Effects of cardiotoxin III on NF-kappa B functions, proliferation and apoptosis in human breast MCF-7 cancer cells. Oncol Res 17:311–321

Das T, Bhattacharya S, Halder B, Biswas A, DasGupta S, Gomes A et al (2011) Cytotoxicity and antioxidant property of a purified fraction (NN-32) of Indian *Naja naja* venom on Ehrlich ascites carcinoma in BALB/c mice. Toxicon 57:1–8

de Lima DC, Abreu PA, de Freitas CC, Santos DO, Borges RO, dos Santos TC, Cabral LM, Rodrigues CR, Castro HC (2005) Snake venom: any clue for antibiotics and CAM? eCAM 2:39–47

Debnath A, Saha A, Gomes A, Biswas S, Chakrabarti P, Giri B, Biswas AK, Dasgupta S, Gomes A (2010) A lethal cardiotoxic-cytotoxic protein from the Indian monocellate cobra (*Naja kaouthia*) venom. Toxicon 56:569–579

Dolati A, Imanieh I, Salehi F, Farahani F (2011) The effect of cysteine on electrodeposition of gold nanoparticle. Mat Sci and Eng B 176:1307–1312

Fan J, Chen S, Gao Y (2003) Coating gold nanoparticles with peptide molecules via a peptide elongation approach. Colloids and Surfaces B: Biointerfaces 28:199–207

Faraji AH, Wipf P (2009) Nanoparticles in cellular drug delivery. Bioorg Med Chem 17:2950–2962

Ghiringhelli F, Puig PE, Roux S, Parcellier A, Schmitt E, Solary E et al (2005) Tumor cells convert immature myeloid dendritic cells into TGF-β-secreting cells inducing CD4+ CD25+ regulatory T cell proliferation. J Exp Med 202:919–929

Ghosh P, Han G, De M, Kim CK, Rotello VM (2008) Gold nanoparticles in delivery applications. Adv Drug Deliver Rev 60:1307–1315

Giri B, Gomes A, Debnath A, Saha A, Biswas AK, Dasgupta SC et al (2006) Antiproliferative, cytotoxic and apoptogenic activity of Indian toad (*Bufo melanostictu*s, Schneider) skin extract on U937 and K562 cells. Toxicon 48:388–400

Gomes A, Roy Choudhury S, Saha A, Mishra R, Giri B, Biswas AK, Debnath A, Gomes A (2007) A heat stable protein toxin (drCT-I) from the Indian Viper (*Daboia russelli russelli*) venom having antiproliferative, cytotoxic and apoptotic activities. Toxicon 49:46–56

Gomes et al (2010) Anticancer potential of animal venoms and toxins. Ind J Exp Biol 48:93–103

Heise PJ, Maxson LR, Dowling HG, Hedges SB (1995) Higher-level snake phylogeny inferred from mitochondrial DNA sequences of 12s rRNA genes. Mol Biol Evol 12:259–265

Higuchi M, Ushiba K, Kawaguchi M (2007) Structural control of peptide-coated gold nanoparticle assemblies by the conformational transition of surface peptides. J Colloid Interface Sci 308:356–363

Holm M, Thomson M, Hoyer M, Hokland P (1998) Optimization of a flow cytometric method for the simultaneous measurement of cell surface antigen, DNA content and in vitro BrdU incorporation into normal and malignant hematopoietic cells. Cytometry 32:28–36

Hosta L, Pla-Roca M, Arbiol J, Iglesias CL, Samitier J, Cruz LJ et al (2009) Conjugation of Kahalalide F with gold nanoparticles to enhance in vitro antitumoral activity. Bioconjugate Chem 20:138–146

Hu CMJ, Zhang L (2012) Nanoparticle-based combination therapy toward overcoming drug resistance in cancer. Biochem Pharmacol 83:1104–1111

Hui RC, Francis RE, Guest SK, Costa JR, Gomes AS, Myatt SS et al (2008) Doxorubicin activates FOXO3a to induce the expression of multidrug resistance gene ABCB1 (MDR1) in K562 leukemic cells. Mol Cancer Ther 7:670–678

Jayat C, Ratinaud MH (1993) Cell cycle analysis by flow cytometry: principles and applications. Biol Cell 78:15–25

Kaufmann SH, Hengartner MO (2011) Pogrammed cell death: alive and well in the new millennium. Trends Cell Biol 11:526–534

Laemmli UK (1970) Cleavage of structural proteins during the assembly of the head of bacteriophage T4. Nature 227:680–685

Lin PJ, Yang SJ, Lee WJ, Hsieh TW, Chung GJ (2006) Berberine induces cell cycle arrest and apoptosis in human gastric carcinoma SNU-5 cell line. World J Gastroenterol 12:21–28

Liu Y, Shipton MK, Ryan J, Kaufman ED, Franzen S, Feldheim DL (2007) Synthesis, stability, and cellular internalization of gold nanoparticles containing mixed peptide-poly(ethylene glycol) monolayers. Anal Chem 79:2221–2229

Lowry OH, Rosebrough NJ, Farr AL, Randall RJ (1951) Protein measurement with the folin phenol reagent. J Biol Chem 193:265–275

Luo H, Li J, Chen X (2009) Antitumor effect of *N*-succinyl-chitosan nanoparticles on K562 cells. Biomed Pharmacother 64:521–526

Newman DJ, Cragg GM, Snader KM (2003) Natural products as sources of new drugs over the period 1981–2002. J Nat Prod 66:1022–1037

Olmedo I, Araya E, Sanz F, Medina E, Arbiol J, Toledo P, Alvarez-Lueje A, Giralt E, Kogan J (2008) How changes in the sequence of the peptide CLPFFD-NH2 can modify the conjugation and stability of gold nanoparticle and their affinity for β-amyloid fibrils. J Am Chem Soc 128:1154–1162

Palma E, Leporatti S, de Luca E, di Renzo N, Mafia M, Ganbacorti-Passerini C et al (2010) Imatinib-loaded polyelectrolyte micro-capsules for sustained targeting of BCR-ABL+ leukemia stem cells. Nanomedicine (Lond) 5:419–431

Ross JS, Linette GP, Stec J, Ross MS, Anwar S, Boguniewicz A (2003) DNA ploidy and cell cycle analysis in breast cancer. Am J Clin Pathol 120:S72–S84

Roy S, Besra SE, De T, Banerjee B, Mukherjee J, Vedasiromoni JR (2008) Induction of apoptosis in human leukemic cell lines U937, K562 and HL-60 by *Litchi chinensis* leaf extract via activation of mitochondria mediated caspase cascades. The Open Leukemia J 1:1–14

Sahoo SK, Labhasetwar V (2005) Enhanced anti-proliferative activity of transferring conjugated paclitaxel loaded nanoparticle is mediated via sustained intracellular drug retention. Mol Pharm 2:373–383

Samal KA, Sreeprasad ST, Praddep T (2010) Investigation of role of NaBH$_4$ in the chemical synthesis of gold nanorods. J Nanopart Res 12:1777–1786

Sargent MJ, Taylor GC (1989) Appraisal of the MTT assay as a rapid test of chemosensitivity in acute myeloid leukaemia. Br J Cancer 60:206–210

Sau TK, Pal A, Jana NR, Wang ZL, Pal T (2001) Size controlled synthesis of gold nanoparticles using photo chemically prepared seed particles. J Nanopart Res 3:257–261

Shapiro GI, Harper JW (1999) Anticancer drug targets: cell cycle and checkpoint control. J Clin Invest 104:1645–1653

Shi W, Sahoo Y, Swihart MT (2004) Gold nanoparticles surface-terminated with bifunctional ligands. Coll Surf A Physicochem Eng Aspects 246:109–113

Sobczak-Kupiec A, Malina D, Zimowska M, Wzorek Z (2011) Characterization of gold nanoparticle for various medical application. Dig J Nanomat Biostruc 6:803–808

Thatte U, Bagadey S, Dahanukar S (2000) Modulation of programmed cell death by medicinal plant. Cell Mol Biol 46:199–214

Tiwari PM, Vig K, Dennis VA, Singh SR (2011) Functionalized gold nanoparticles and their biomedical applications. Nanomaterials 1:31–63

Tong XH, Lin SG, Fujii M, Hou DX (2004) Molecular mechanisms of echinocystic acid induced apoptosis in HepG2 cells. Biochem Biophys Res Commun 321:539–546

Triulzi RC, Dai Q, Zoub J, Leblanc RM, Gud Q, Orbulescu J, Huob Q (2008) Photothermal ablation of amyloid aggregates by gold nanoparticles. Coll Surf B Biointerf 63:200–208

Tu AT (1988) Snake venoms: general background and composition. Venoms chemistry and molecular biology. Wiley, New York, pp 1–19

Wang X, Wang Y, Chen ZG, Shin DM (2009) Advances of cancer therapy by nanotechnology. Cancer Res Treat 41:1–11

Yang X, Koh CG, Liu S, Pan X, Santhanam R, Yu B et al (2009) Transferring receptor targeted lipid nanoparticles for delivery of an antisense oligodeoxyribonucleotide against Bcl-2. Mol Pharm 6:221–230

Zhang L, Cui L (2007) A cytotoxin isolated from agkistrodon acutus snake venom induces apoptosis via Fas pathway in A549 cells. Toxicol In Vitro 21:1095–1103

Zubarev RE, Xu J, Sayyad A, Gibson DJ (2006) Amphiphilic gold nanoparticles with V-shaped arms. J Am Chem Soc 128:4959–4974